

Die Grenzen der
Chemie neu ausloten?
It takes
#HumanChemistry

Wir suchen kreative Chemikerinnen und Chemiker,
die mit uns gemeinsam neue Wege gehen wollen –
mit Fachwissen, Unternehmertum und Kreativität für
innovative Lösungen. Informieren Sie sich unter:

evonik.de/karriere

Oxidation and Hot Gas Corrosion of Al–Cr–Fe–Ni-Based High-Entropy Alloys with Addition of Co and Mo

Katharina Nicole Gabrysiak,* Uwe Gaitzsch, Thomas Weißgärber, and Bernd Kieback

Multicomponent, high-entropy alloys (HEAs) are promising candidates for replacing conventional alloys in high-temperature applications. Herein, the high-temperature corrosion of AlCrFeNiX_{0.5} (X = Co, Mo) is investigated. The samples are tested for their oxidation resistance at temperatures up to 1200 °C for 120 h and their behavior in NaCl/Na₂SO₄ at 900 °C for 96 h. They are benchmarked against commercial alloys such as FeCrAl. Despite the same contents of Al and Cr, the HEAs form different oxide layers showing very different oxidation resistance. The type of oxide is related to the multiphase microstructure. The samples exhibit different amounts of ordered and unordered body-centered cubic (bcc) phase. The Co-containing specimen shows an oxidation resistance that performs similarly well as FeCrAl. Its behavior is ascribed to the formation of an Al₂O₃ layer, which is very stable at high temperatures. The sample with X = Mo exhibits an additional Mo-rich sigma phase, thus posing the risk of catastrophic oxidation. However, the Mo-containing HEA is more resistant in the environment of molten salt. Preoxidation treatment at a lower oxygen partial pressure proves to prolong life span of the Mo-containing HEA in hot air. Furthermore, a positive impact on oxidation resistance by addition of Y is affirmed.

relevance for high-temperature applications are assumed, such as sluggish diffusion,^[1–5] high-temperature phase stability,^[2,6,7] and creep strength.^[7–13] Currently, some of them are controversially discussed (e.g., sluggish diffusion^[14–16]). The concept of multicomponent alloys offers many opportunities in alloy design such as high amounts of Al and Cr for corrosive environments.

In this article, Al–Cr–Fe–Ni-based HEAs alloyed with Mo or Co are investigated. Cr and Al are known to form oxides with excellent chemical stability. Co is a base element for several high-temperature alloys, whereas Mo is used to alloy steels and superalloys to increase creep strength. Mo-containing alloys require particular protection, since its oxides are volatile.^[17] In addition, Y is added, which is known to stabilize alumina layers.^[18,19]

AlCoCrFeNi has been extensively researched concerning: thermal properties,^[20] mechanical properties depending on the Al content,^[21–23] also at elevated temperatures,^[10,20,24] and precipitation hardening.^[24–28] However, the HEA AlCrFeMoNi is almost not investigated. Mo was reviewed as an element in refractory HEAs^[29–31] or as an additional component in AlCoCrFeNi.^[9,27,32–36] Also, the comprehensions of oxidation behavior and mechanism models for multicomponent alloys in general are lacking. In contrast, the advantage of high Al contents in different HEAs was verified experimentally.^[37–41] The oxidation rate constant of alumina forming HEAs is within the range of conventional alumina formers,^[37,41] although the results may be affected by spallation.


Most of these studies were executed below 1000 °C or were performed with thermogravimetric approaches for short periods of time. Many materials start to weaken only above this temperature. For demanding applications in varying environments, such as biomass power plants, high-temperature alloys are urgently needed. Therefore, this article presents the exposure in air at 1200 °C for 120 h. The results are compared to commercial high-temperature alloys such as FeCrAl and Inconel alloys. The microstructure of three as-cast and oxidized HEAs (AlCo_{0.5}CrFeNi, AlCrFeMo_{0.5}Ni, and AlCrFeMo_{0.5}Ni+Y) was studied with focus on the relation between initial state and oxidation mechanism. Also, the resistance against sulfate-induced hot gas corrosion as well as preoxidation at lowered oxygen partial pressure is assessed for the first time.

1. Introduction

High-entropy alloys (HEAs) are composed of multiple components in equiatomic or nearly equiatomic concentrations. In addition to solid solution hardening, further properties with

K. N. Gabrysiak, Dr. U. Gaitzsch, Dr. T. Weißgärber, Prof. B. Kieback
Sintered Materials
Fraunhofer Institute for Manufacturing Technology and Advanced Materials (IFAM Dresden)
Winterbergstr. 28, Dresden 01277, Germany
E-mail: k.n.gabrysiak@ifw-dresden.de

K. N. Gabrysiak
Alloy Design and Processing
Leibniz Institute for Solid State and Materials Research (IFW Dresden)
Helmholtzstr. 20, Dresden 01069, Germany

 The ORCID identification number(s) for the author(s) of this article can be found under <https://doi.org/10.1002/adem.202100237>.

© 2021 The Authors. Advanced Engineering Materials published by Wiley-VCH GmbH. This is an open access article under the terms of the Creative Commons Attribution-NonCommercial-NoDerivs License, which permits use and distribution in any medium, provided the original work is properly cited, the use is non-commercial and no modifications or adaptations are made.

DOI: 10.1002/adem.202100237

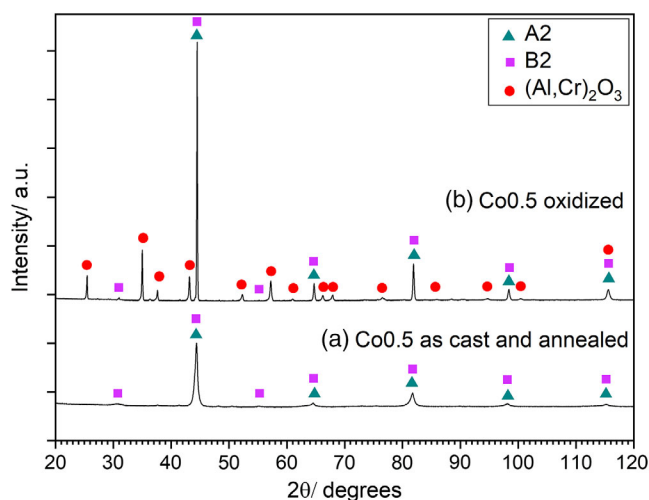


Figure 1. a,b) XRD pattern of Co0.5 before and after oxidation.

2. Results

2.1. Microstructure of the As-Cast Samples

After casting, all alloys exhibit a multiphase microstructure. AlCo_{0.5}CrFeNi (Co0.5) shows a body-centered cubic (bcc) solid solution phase, called A2 (*Im* $\bar{3}$ *m*, Nr. 229), and an ordered bcc phase, B2 (*Pm* $\bar{3}$ *m*, Nr. 221). The crystal structure, examined by X-ray diffraction (XRD), is shown in Figure 1a. Al and Ni are enriched in the B2 phase, whereas increased amounts of Cr and Fe can be determined in the A2 phase (see Figure 2). Co is less selective but shows an enrichment in the B2 phase. The A2 phase constitutes a continuous network as well as small precipitates in the B2 grains formed by spinodal decomposition. The spinodal decomposition is well-known in Al–Co–Cr–Fe–Ni HEAs.^[20,21,42]

Co0.5 shows a microstructure that is very similar to that of equimolar AlCoCrFeNi.^[20,21,43,44] This also corresponds to thermodynamic estimations. Regarding binary mixing enthalpies

as an indication for binding affinity, Al and Ni exhibit the minimum value of $\Delta H_{\text{mix}} = -22 \text{ kJ mol}^{-1}$ among the elements.^[45] Furthermore, there is a high affinity between Al and Co ($\Delta H_{\text{mix}} = -19 \text{ kJ mol}^{-1}$ ^[45]), so that Co can occupy the lattice sites of Ni in B2.^[46] The mixing enthalpies between Co, Cr, and Fe are close to zero,^[45] so that the mixing entropy becomes dominant and they can form a solid solution. The volume ratio of A2 and B2, identified by gray scale analysis, is $\approx 2:3$.

AlMo_{0.5}CrFeNi (Mo0.5) has a similar microstructure in which Mo is enriched in the A2 phase (see Figure 3). For this reason, the percentage of A2 increases by 15% (A2:B2 in the ratio of 11:8). In addition, a Mo-rich network was found at the former solidification front. The network further consists of Cr and Fe (see Figure 3). In accordance with literature,^[27,35,42] the Mo-rich network can be attributed to the sigma phase due to its composition. Grain size refinement and phase distribution alteration, such as avoiding a Mo-rich network, can be realized by using powder metallurgy fabrication. Mo0.5 and AlMo_{0.5}CrFeNi-Y (Mo0.5-Y) display the same microstructure, i.e., no influence of yttrium on the microstructure can be determined.

2.2. Isothermal Oxidation

After isothermal oxidation in air, Co0.5 forms a stable alumina layer (α -Al₂O₃) with partial solution of Cr. The growth rate of the layer decreases after $\approx 70 \text{ h}$ due to diffusion-controlled oxidation. It reaches a thickness of 4.2 μm after 120 h at 1200 °C as measured by scanning electron microscopy (SEM) (Figure 4). Even though Co0.5 forms a protective oxide, attention should be paid to layer adhesion. As shown in Figure 5, cracks between the bulk material and the oxidized surface as well as within the surface layer can be found.

The cracks result from internal stress induced by two main mechanisms. First, the different lattice parameters of the substrate and Al₂O₃. The larger molar volume of Al₂O₃ can lead to compression stress during the oxide growth within the layer. This can cause bulging and spallation. The second mechanism is thermal stress

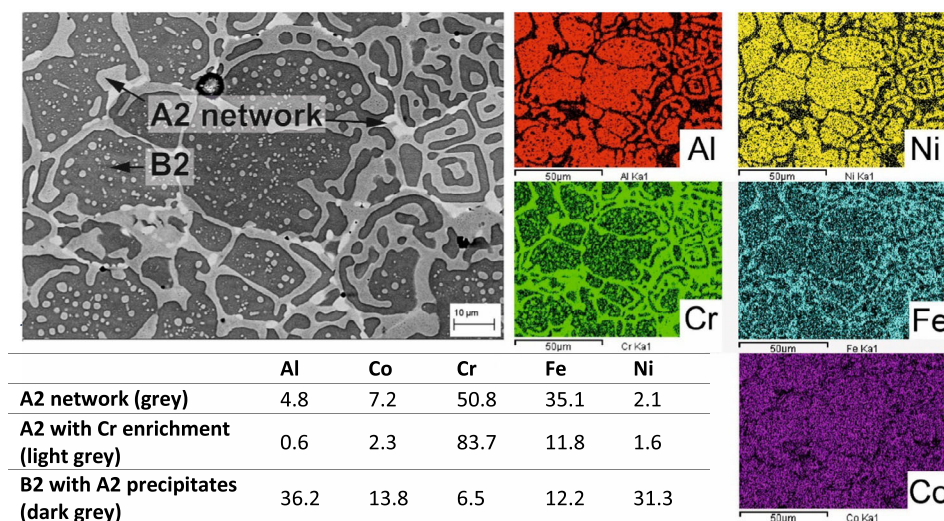


Figure 2. Microstructure (BSE) of Co0.5, mapping and local composition in at% measured by EDS, (please note that the volume of excitation exceeds the size of the phases).

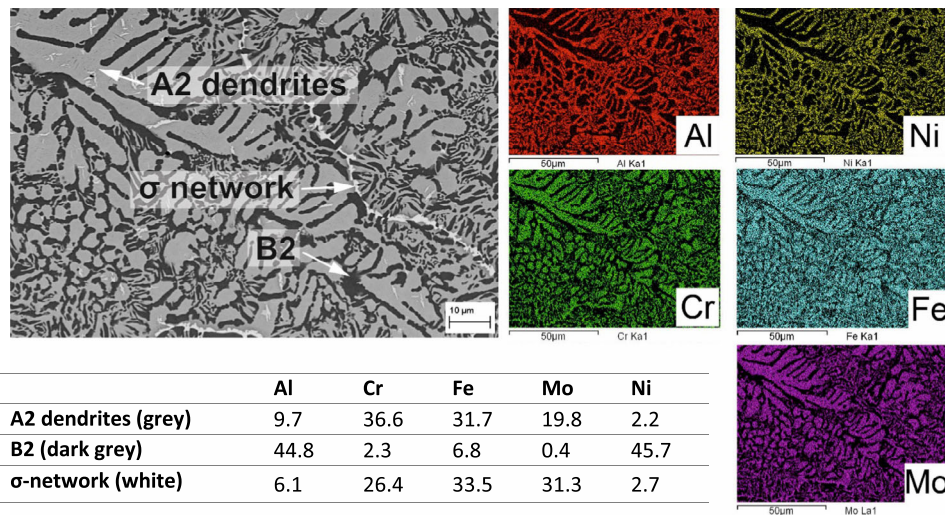


Figure 3. Microstructure (BSE) of Mo0.5-Y, mapping and local composition in at% measured by EDS (please note that the volume of excitation exceeds the size of the phases).

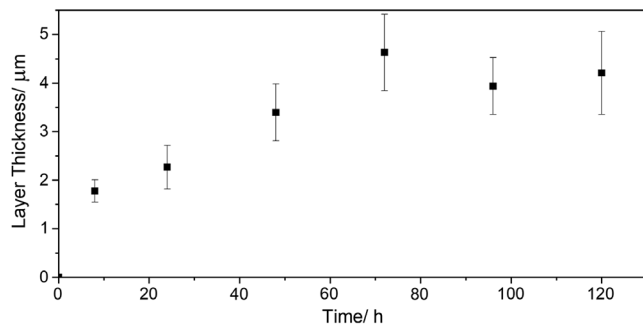


Figure 4. Oxide growth measured by SEM and standard deviation of Co0.5 during isothermal oxidation at 1200 °C (at least 15 measurement points per layer).

during cooling, which results from different coefficients of thermal expansion. Oxide layers have a high ionic bond content, and

therefore, they shrink less than the substrate during cooling. After spallation, previously unexposed surface oxidizes. For this reason, the thickness of oxide layers (see Figure 4) might be slightly underestimated.

The issue of spallation and repassivation becomes particularly clear during cyclic oxidation (not discussed in detail) by forming an Al depletion zone below the oxide layer (see Figure 6). Consequently, the formation of Cr oxide during long-time cyclic oxidation is probable.

The Mo-containing HEAs are not stable in hot air due to the formation of volatile Mo oxides (MoO_3 and MoO_2). Mixed (Al,Cr, Fe,Ni)-oxides are formed in an early stage of oxidation (see Figure 7b,c) and cannot protect the sample sufficiently. This catastrophic oxidation causes the disintegration of the whole sample due to a selective attack of the Mo-enriched network. After failure, the entire cross section was found to be oxidized without any presence of Mo (see Figure 8). The failure of Mo0.5-Y appears significantly later compared to the Mo0.5 samples. The Y-free

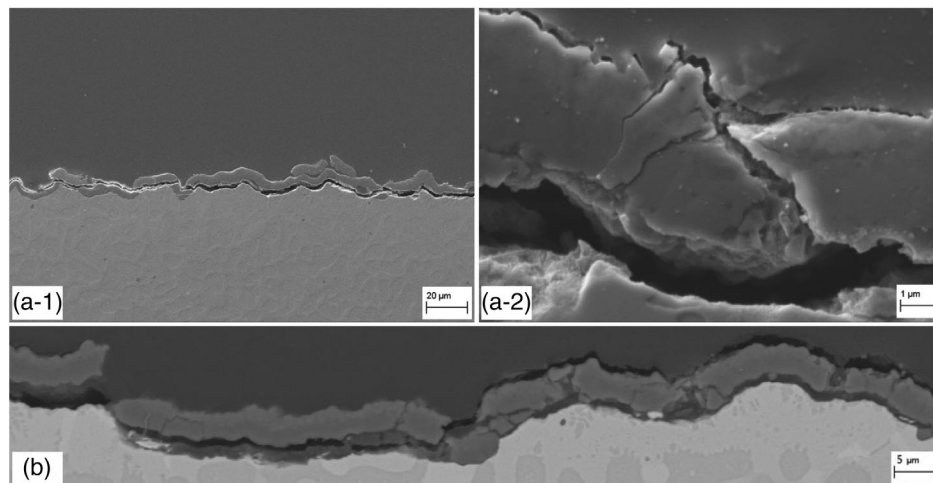


Figure 5. a) Co0.5 after 72 h and b) 120 h of oxidation at 1200 °C (SE): cracks within oxide and along the interface, spalling, and repassivation.

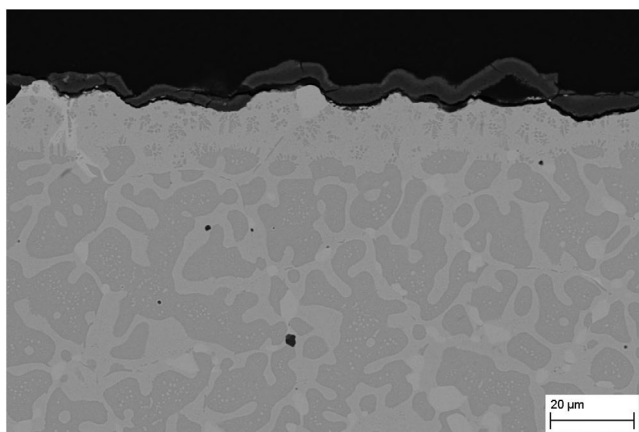


Figure 6. Co0.5 after 120 h of cyclic oxidation (six cooling cycles) with a B2 depletion zone beneath the oxide layer.

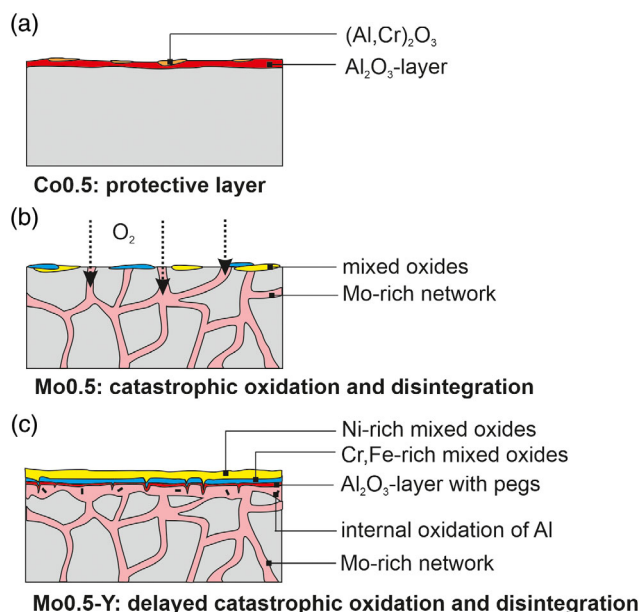


Figure 7. Schematic oxidation for a) Co0.5, b) Mo0.5, and c) Mo0.5-Y at 1200 °C after completed layer formation.

samples collapse after less than 4 h whereas Mo0.5-Y lasts more than 30 h demonstrating the positive impact of yttrium.

The formation of a closed protective Al₂O₃ layer is not possible due to kinetic reasons: the amount of Al-rich B2 phase is 20% less in Mo0.5 comparing to Co0.5. In addition, the microstructure of Mo0.5 displays large dendrites of the A2 phase (see Figure 3). Consequently, the diffusion path for Al is longer and the formation of Al₂O₃ inhibited.

Y has a positive effect on the resistance against oxidation. At an early stage, Mo0.5-Y forms Ni-rich oxides, since they are kinetically favored (see Figure 9). This leads to higher concentrations of Fe and Cr, resulting in a Fe-, Cr-rich oxide layer (e.g., FeCr₂O₄). Beneath this layer, the oxygen partial pressure decreases to the extend that a thin Al₂O₃ layer can grow. The alumina layer with pegs, presumably promoted by yttrium, protects the HEA from catastrophic oxidation for a short time. Nevertheless, the oxides, in particular the thicker mixed oxide layer, lead to stress within the layers and on the interfaces of Mo0.5-Y. Through spallation and insufficient density of the layers, oxygen reacts with the Mo-enriched zone below the oxides. It still can be shown that Y promotes the formation of protective layers and their stronger adhesion in the HEAs as already known from literature.^[19]

In comparison with the commercial alloys, Co0.5 proves its high resistance to isothermal oxidation by forming the thinnest oxide layer in this study (see Table 1), together with FeCrAl. Both layers consist of Al₂O₃, which is known to have a very small growth rate (low parabolic rate constant). However, Co0.5 and FeCrAl suffer from spallation. The Cr-oxide formers were less stable (NiCr23Fe, X10NiCrAlTi32-21, and NiCr22Mo9Nb). High growth rates and double layers with mixed oxides were found to be present in these alloys. Their true impact zone is a lot larger than the measured thickness of oxidation layers due to pores, major depletion zones, as well as inner corrosion. In general, it is well known that Cr₂O₃ is not long-term stable at 1200 °C.^[47] It grows faster than Al₂O₃ and it tends to evaporation.

2.3. Preoxidation of Mo0.5

Since the formation of a protective oxide layer on Mo0.5 and Mo0.5-Y in air is kinetically not possible, the HEAs were preoxidized under wet hydrogen. The resulting oxygen partial pressure of the atmosphere was chosen to be lower than the equilibrium oxygen dissociation pressure of the Ni, Co, Mo, and Fe oxides.

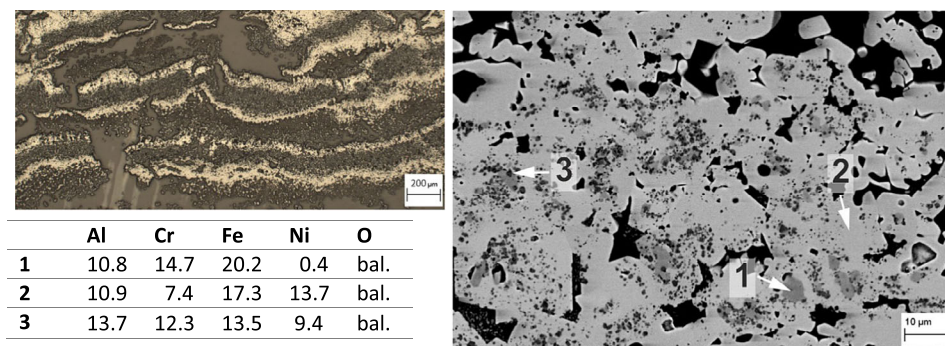


Figure 8. Residuals of Mo0.5-Y after 52 h of oxidation at 1200 °C, optical microscopy, and BSE picture with EDS.

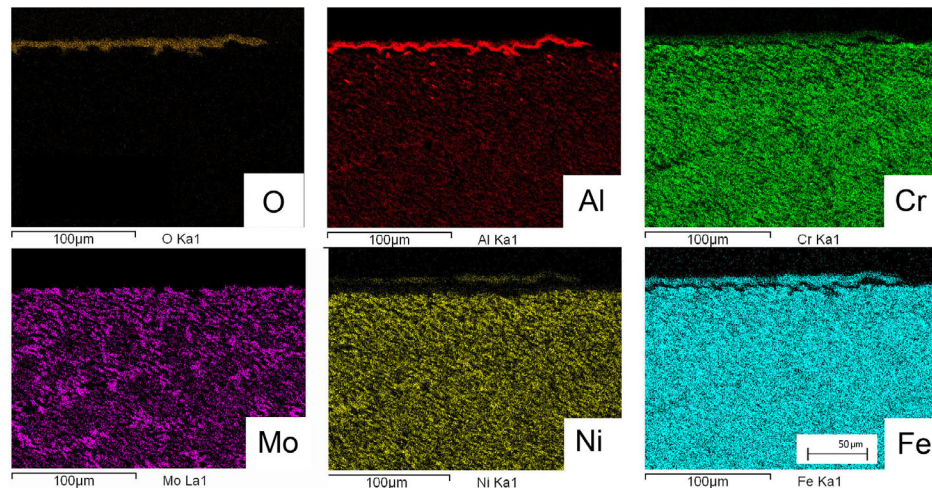


Figure 9. EDS mapping of Mo0.5-Y after 30 h of oxidation at 1200 °C, from top to substrate: Ni-rich oxides, Cr,Fe-rich oxides, Al oxide with pegs, Mo-enrichment under the oxide layers.

Table 1. Thickness and morphology of oxide layers and standard deviation of Co0.5 and reference alloys after oxidation at 1200 °C for 120 h (at least 15 measurement points per layer).

Alloy	Outer layer [μm]	Inner layer [μm]	Morphology
Co0.5	4.21 ± 0.19	None	(Al,Cr) ₂ O ₃ -layer with spallation
FeCrAl	6.26 ± 0.26	None	Al ₂ O ₃ -layer with spallation
NiCr23Fe	17.07 ± 1.45	23.21 ± 1.09	Spallation of impure Cr ₂ O ₃ layer, internal oxidation of Al, pores beneath the layer
X10NiCrAlTi32-21	18.85 ± 1.25	20.99 ± 1.15	Spallation of impure Cr ₂ O ₃ -/FeCr ₂ O ₄ layer, internal oxidation of Al, pores beneath the layer
NiCr22Mo9Nb	67.89 ± 2.56	12.29 ± 1.24	Spallation of impure Cr ₂ O ₃ -/CrNbO ₄ layer, further mixed oxides, pores beneath the layer, significant Cr-depletion zone

Therefore, the formation of mixed oxides is suppressed and only the oxides of Al and Cr are thermodynamically stable. As expected, Co0.5 forms an alumina layer with local Cr enrichment just as in air (see **Figure 10a**). Mo0.5 and Mo0.5-Y exhibit a closed layer of Cr₂O₃ and internal oxidation of Al underneath (see **Figure 10b,c**). Al is enriched in the B2 phase, which does not form a continuous network. Therefore, aluminum diffusion into the A2 phase is necessary to form a protective layer. Also, the fraction of Cr-rich A2 phase is higher in the Mo-containing HEAs. Due to shorter diffusion paths, the formation of Cr₂O₃ is favored. The oxygen partial pressure underneath the Cr oxide is still high enough to allow the oxidation of aluminum.

A possible mechanism for extended oxidation may be as follows: the fragments of internal oxidation grow until Al₂O₃ forms

a closed bottom oxide layer underneath the Cr oxide. Subsequently, the oxidation is defined by the growth of Al₂O₃. Cr₂O₃ stays nearly unaffected during further exposure due to the spatial separation of the chromium metal reservoir. The differences in microstructure of Mo0.5 and Mo0.5-Y result from variation in cooling within the samples. In the examined sections (see **Figure 10b,c**) Mo0.5 has the finest structural features in the range of 1–3 μm, so that the bottom Al₂O₃ layer is already closed after 1 h. A further gain of the suppression of mixed oxides is the absence of Mo enrichment below the interface. The preoxidation prolongs the lifetime of the Mo-containing HEAs (see also hot gas corrosion), although further studies are necessary for quantitative conclusions. In practice, the protective effect is also limited due to the risk of spallation.

2.4. Hot Gas Corrosion

Preoxidation did not affect the hot gas corrosion behavior of Co0.5, but it improved the performance of the Mo containing alloys. They remain stable during the entire testing duration of 96 h and exhibit relatively low depth of corrosion attack. Different oxides were determined by energy dispersive X-ray spectroscopy (EDS) on the surface of Co0.5. From top to substrate, FeCr₂O₄, Cr₂O₃, and Al₂O₃ were found. Furthermore, a significant depletion zone of Al and Cr up to 200 μm, a network of pores, a selective attack on the A2 phase, as well as CrS were identified (see **Figure 11**).

In the first step, the molten salt dissolves the protective oxides which precipitate on the liquid–air interface. Next, internal corrosion occurs via the formation of sulfides. CrS is more stable comparing to other sulfides as Ni₃S₂ which forms a eutectic with Ni at 645 °C.^[48] Therefore, high amounts of Cr are necessary to absorb S. Nevertheless, the corrosion depth increases further due to the oxidation of the sulfides and thus the release of elemental S within the sample. The depth reaches locally more than 250 μm for Co0.5 after 96 h of hot gas corrosion (see **Figure 11**).

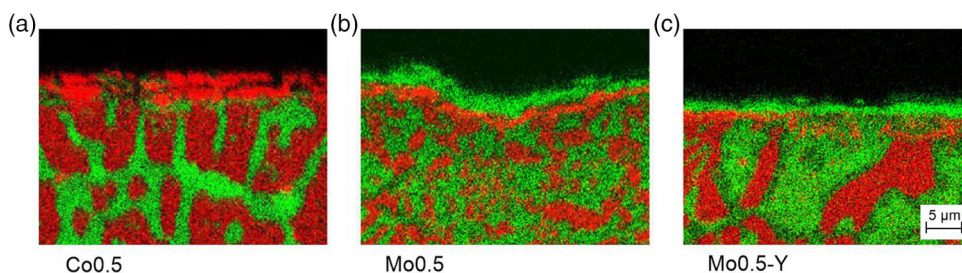


Figure 10. EDS mapping for a) Co0.5, b) Mo0.5 and c) Mo0.5-Y after preoxidation in wet hydrogen at for 1 h, Al: red, Cr: green.

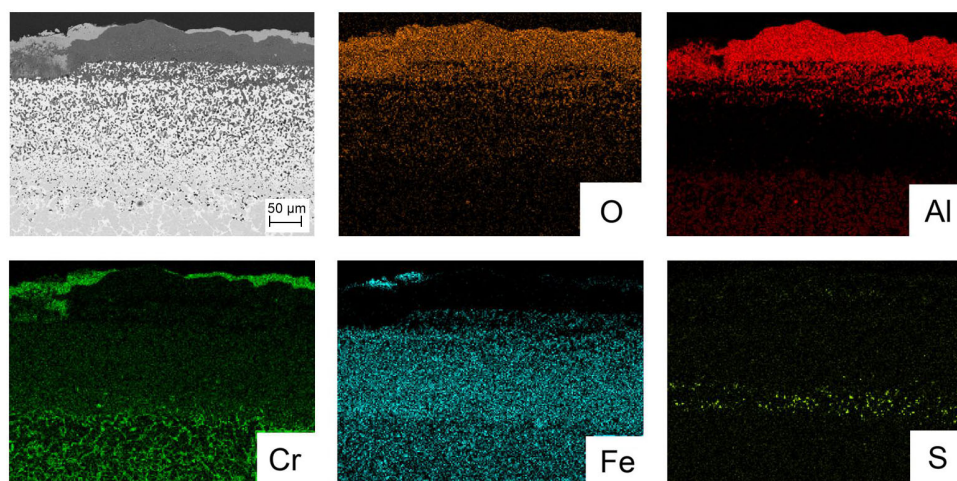


Figure 11. Microstructure (BSE) image of Co0.5 and mapping of oxide forming elements and sulfur after 96 h of hot gas corrosion.

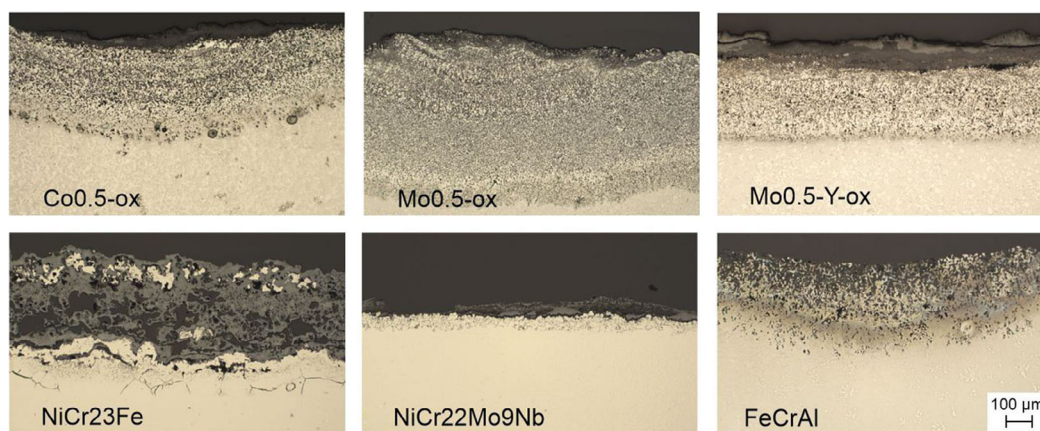


Figure 12. Corrosion layers and locally high depths of attack, as-cast, and preoxidized HEAs and reference alloys by optical microscope.

NiCr22Mo9Nb (IN 625) shows the lowest corrosion depth of all samples (see **Figure 12**). Among Cr, also Mo and Nb form stable sulfides and thus getter the S. As shown in **Figure 12**, Mo0.5-Y has the lowest corrosion rate among the HEAs because of its ability to getter S by Cr, Mo, and Y.

3. Conclusion

In this study, the microstructures as well as the oxidation and hot gas corrosion behavior of AlCrFeNiX_{0.5} (X = Co, Mo) were investigated. The following conclusions can be drawn as follows:

Table 2. Overall composition of HEAs measured by XRF with standard deviation of six samples and EDS (in brackets) in at%.

Alloy	Abbreviation	Al	Co	Cr	Fe	Mo	Ni	Y
AlCo _{0.5} CrFeNi	Co0.5	24.3 ± 2.5 (25.2)	11.5 ± 0.6 (12.3)	23.9 ± 0.7 (22.1)	19.3 ± 0.7 (18,8)	–	20.7 ± 0.9 (21,1)	–
AlCrFeMo _{0.5} Ni	Mo0.5	24.2 ± 1.1 (23.9)	–	21.3 ± 0.4 (22,4)	21.2 ± 0.3 (21.2)	10.8 ± 0.3 (11.8)	22.6 ± 0.3 (20.8)	–
AlCrFeMo _{0.5} Ni+Y	Mo0.5-Y	23.6 ± 2.7 (24.7)	–	21.0 ± 0.8 (20.7)	21.8 ± 0.9 (21.0)	11.1 ± 0.3 (11.4)	22.5 ± 0.8 (22.1)	– ^{a)}

^{a)}700 ppm regarding to nominal composition.

1) AlCo_{0.5}CrFeNi exhibits the Al, Ni-enriched, ordered main phase B2 and the Cr, Fe-enriched second phase A2. In AlMo_{0.5}CrFeNi, the A2 phase dominates by high solubility of Mo. Also, a third phase, the Mo-rich sigma phase, was determined to form a continuous network. 2) Despite same amounts of Al and Cr, disparate types of oxide layers are formed due to the differences in microstructure. In AlCo_{0.5}CrFeNi, the Al diffusion path is short enough to form a stable, dense Al₂O₃ layer making it the sample with the lowest oxidation rate in this study. The layer has a thickness of 4.2 μm after 120 h at 1200 °C. In AlMo_{0.5}CrFeNi, mixed oxides were found in an early stage of oxidation. As they do not provide enough protection, the Mo-containing HEAs suffer from catastrophic oxidation of the Mo-rich network. 3) The investigation of the Mo-containing HEAs demonstrates the positive impact of yttrium by promoting the formation of Al₂O₃. The behavior of AlMo_{0.5}CrFeNi+Y indicates improvements in layer adhesion and life span. The layer adhesion of AlCo_{0.5}CrFeNi might be also improved by addition of Y. 4) Preoxidation under low oxygen partial pressure is proposed to protect the Mo-containing HEAs from catastrophic oxidation. Due to the higher amount of Cr-containing A2 phase, a protective oxide layer of Cr₂O₃ with Al₂O₃ below forms on the surface of AlMo_{0.5}CrFeNi(+Y). 5) In contrast to high-temperature oxidation, high amounts of Cr and Mo are beneficial against hot gas corrosion. For this reason, AlMo_{0.5}CrFeNi+Y is more resistant against S. The reference alloy NiCr22Mo9Nb exhibits the minimal hot gas corrosion depth, but has the highest oxidation rate in this study. 6) In conclusion, the formation of oxide layers in multicomponent alloys can be very different depending on the microstructure, in particular the type of phases, the structure size, and the amount of phases. They do not follow oxidation maps, which mainly consider the amounts of Al and Cr. There were no HEA-specific effects on oxidation detected. 7) Finally, the detected properties make especially AlCo_{0.5}CrFeNi an interesting candidate for demanding applications (e.g., biomass power plants). The use of chromia formers such as AlMo_{0.5}CrFeNi+Y can also be advantageous due to their good resistance against hot gas corrosion. Preoxidation is crucial to achieve a maximum service lifetime.

4. Experimental Section

The HEAs were produced by induction melting of raw materials (purity > 99%) under argon atmosphere (700 mbar). The overall compositions are shown in Table 2. For homogenization, the alloys were heat-treated at 1200 °C for 48 h in argon atmosphere (1 bar). Each bulk sample was sandblasted and cut into cylinders (diameter: 13.6 mm, height: 2.5 mm). The results of oxidation were compared to the following purchased standard high-temperature alloys: FeCrAl (1.4767), Alloy 800

(X10NiCrAlTi32-20, 1.4876), Alloy 625 (NiCr22Mo9Nb, 2.4856), and Alloy 601 (NiCr23Fe, 2.4851).

The oxidation behavior was tested at 1200 °C in an air furnace for 120 h. The samples were placed into alumina crucibles with alumina granules. The thickness of the oxide layers was measured at continuously oxidized samples with SEM. For each heating period, one sample was removed from the oven and examined at three different areas with at least five measurements per area. Preoxidation took place in wet hydrogen (2.3 vol% water) at 1000 °C for 1 h.

To investigate the hot gas corrosion, the samples were coated in the as-cast and the preoxidized state with a solution of NaCl/Na₂SO₄ (weight fraction 1:3). The composition allowed the eutectic formation with a melting point of 625 °C^[49] in the furnace. The samples were dried on a hot plate at 200 °C and subsequently exposed in an air furnace at 900 °C. After 24 h of exposure, the samples were removed, mechanically cleaned (brushed and washed by ultrasonic bath), and inspected visually. Next, the samples were recoated and placed back into the air furnace. This cycle was repeated four times for a total testing duration of 96 h.

Cross sections of the oxidized and corroded specimens were investigated by optical microscopy (MEF 4A Leica Micro-systems) and by SEM (EVO 50 Carl Zeiss) in backscattered electron (BSE) as well as in secondary electron (SE) mode. The composition and mappings were examined by EDS. The overall composition was verified by X-ray fluorescence spectroscopy (XRF, Alpha 8000 LZX Innov-X Systems) of six samples for each cast. The crystal structure of the samples and the oxide layer was analyzed by XRD (D8 Advance Bruker) with Cu Kα radiation.

Acknowledgements

Funding by the German Federal Ministry for Food and Agriculture, Grant no. 22404815, is greatly acknowledged. The authors thank Hans Dietrich Böhm and Arne Boden for conducting the high-temperature experiments and Thomas Wittig for operating the induction melting device.

Open access funding enabled and organized by Projekt DEAL.

Conflict of Interest

The authors declare no conflict of interest.

Data Availability Statement

The data that support the findings of this study are available from the corresponding author upon reasonable request.

Keywords

alumina former, chromia former, high-entropy alloys, hot gas corrosion, oxidation, reduced oxygen partial pressure

Received: February 25, 2021
Revised: April 26, 2021
Published online: May 11, 2021

- [1] D. L. Beke, G. Erdélyi, *Mater. Lett.* **2016**, *164*, 111.
- [2] J.-W. Yeh, *Eur. J. Control* **2006**, *31*, 633.
- [3] K.-Y. Tsai, M.-H. Tsai, J.-W. Yeh, *Acta Mater.* **2013**, *61*, 4887.
- [4] K. Kulkarni, G. P. S. Chauhan, *AIP Adv.* **2015**, *5*, 97162.
- [5] J. Dąbrowa, W. Kuczka, G. Cieślak, T. Kulik, M. Danielewski, J.-W. Yeh, *J. Alloys Compd.* **2016**, *674*, 455.
- [6] S. Praveen, J. Basu, S. Kashyap, R. S. Kottada, *J. Alloys Compd.* **2016**, *662*, 361.
- [7] *High-Entropy Alloys* (Eds.: M. C. Gao, J.-W. Yeh, P. K. Liaw, Y. Zhang), Springer International Publishing, Cham **2016**.
- [8] S.-T. Chen, W.-Y. Tang, Y.-F. Kuo, S.-Y. Chen, C.-H. Tsau, T. Shun, J.-W. Yeh, *Mater. Sci. Eng.: A* **2010**, *527*, 5818.
- [9] C.-Y. Hsu, W.-R. Wang, W.-Y. Tang, S.-K. Chen, J.-W. Yeh, *Adv. Eng. Mater.* **2010**, *12*, 44.
- [10] T. Cao, J. Shang, J. Zhao, C. Cheng, R. Wang, H. Wang, *Mater. Lett.* **2016**, *164*, 344.
- [11] D.-H. Lee, M.-Y. Seok, Y. Zhao, I.-C. Choi, J. He, Z. Lu, J.-Y. Suh, U. Ramamurty, M. Kawasaki, T. G. Langdon, J. Jang, *Acta Mater.* **2016**, *109*, 314.
- [12] Y. Ma, Y. H. Feng, T. T. Debela, G. J. Peng, T. H. Zhang, *Int. J. Refract. Met. Hard Mater.* **2016**, *54*, 395.
- [13] W. Li, G. Wang, S. Wu, P. K. Liaw, *J. Mater. Res.* **2018**, *33*, 3011.
- [14] M. Vaidya, S. Trubel, B. S. Murty, G. Wilde, S. V. Divinski, *J. Alloys Compd.* **2016**, *688*, 994.
- [15] D. B. Miracle, *JOM* **2017**, *69*, 2130.
- [16] C. Zhang, F. Zhang, K. Jin, H. Bei, S. Chen, W. Cao, J. Zhu, D. Lv, *J. Phase Equilib. Diffus.* **2017**, *38*, 434.
- [17] C. Wagner, *Angew. Chem., Int. Ed.* **1936**, *49*, 735.
- [18] T. A. Ramanarayanan, R. Ayer, R. Petkovic-Luton, D. P. Leta, *Oxidation Met.* **1988**, *29*, 445.
- [19] G. R. Holcomb, J. Tylczak, C. Carney, *JOM* **2015**, *67*, 2326.
- [20] W.-R. Wang, W.-L. Wang, J.-W. Yeh, *J. Alloys Compd.* **2014**, *589*, 143.
- [21] W.-R. Wang, W.-L. Wang, S.-C. Wang, Y.-C. Tsai, C.-H. Lai, J.-W. Yeh, *Intermetallics* **2012**, *26*, 44.
- [22] Y. Lv, R. Hu, Z. Yao, J. Chen, D. Xu, Y. Liu, X. Fan, *Materials & Design* **2017**, *132*, 392.
- [23] Z. Tang, M. C. Gao, H. Diao, T. Yang, J. Liu, T. Zuo, Y. Zhang, Z. Lu, Y. Cheng, Y. Zhang, K. A. Dahmen, P. K. Liaw, T. Egami, *JOM* **2013**, *65*, 1848.
- [24] M. Chen, L. Lan, X. Shi, H. Yang, M. Zhang, J. Qiao, *J. Alloys Compd.* **2019**, *777*, 180.
- [25] S. Niu, H. Kou, T. Guo, Y. Zhang, J. Wang, J. Li, *Mater. Sci. Eng.: A* **2016**, *671*, 82.
- [26] T. Shun, Y.-C. Du, *J. Alloys Compd.* **2009**, *478*, 269.
- [27] T. Shun, C.-H. Hung, C.-F. Lee, *J. Alloys Compd.* **2010**, *495*, 55.
- [28] T. M. Butler, M. L. Weaver, *J. Alloys Compd.* **2017**, *691*, 119.
- [29] Y. Xiao, W. Kuang, Y. Xu, L. Wu, W. Gong, J. Qian, Q. Zhang, Y. He, *J. Mater. Res.* **2019**, *34*, 301.
- [30] O. N. Senkov, S. V. Senkova, D. M. Dimiduk, C. Woodward, D. B. Miracle, *J. Mater. Sci.* **2012**, *47*, 6522.
- [31] F. Müller, B. Gorr, H.-J. Christ, H. Chen, A. Kauffmann, M. Heilmaier, *Mater. High Temp.* **2018**, *35*, 168.
- [32] C.-Y. Hsu, T.-S. Sheu, J.-W. Yeh, S.-K. Chen, *Wear* **2010**, *268*, 653.
- [33] C.-Y. Hsu, C.-C. Juan, S.-T. Chen, T.-S. Sheu, J.-W. Yeh, S.-K. Chen, *JOM* **2013**, *65*, 1829.
- [34] C.-C. Juan, C.-Y. Hsu, C.-W. Tsai, W.-R. Wang, T.-S. Sheu, J.-W. Yeh, S.-K. Chen, *Intermetallics* **2013**, *32*, 401.
- [35] J. M. Zhu, H. M. Fu, H. F. Zhang, A. M. Wang, H. Li, Z. Q. Hu, *Mater. Sci. Eng.: A* **2010**, *527*, 6975.
- [36] P.-K. Huang, J.-W. Yeh, T.-T. Shun, S.-K. Chen, *Adv. Eng. Mater.* **2004**, *6*, 74.
- [37] T. M. Butler, M. L. Weaver, *J. Alloys Compd.* **2016**, *674*, 229.
- [38] Z. Rao, X. Wang, Q. Wang, T. Liu, X. Chen, L. Wang, X. Hui, *Adv. Eng. Mater.* **2017**, *19*, 1600726.
- [39] Y.-J. Chang, A.-C. Yeh, *J. Alloys Compd.* **2015**, *653*, 379.
- [40] T. M. Butler, J. P. Alfano, R. L. Martens, M. L. Weaver, *JOM* **2015**, *67*, 246.
- [41] S. Wang, Z. Chen, P. Zhang, K. Zhang, C. L. Chen, B. L. Shen, *Vacuum* **2019**.
- [42] A. Munitz, S. Salhov, S. Hayun, N. Frage, *J. Alloys Compd.* **2016**, *683*, 221.
- [43] H. Shiratori, T. Fujieda, K. Yamanaka, Y. Koizumi, K. Kuwabara, T. Kato, A. Chiba, *Mater. Sci. Eng.: A* **2016**, *656*, 39.
- [44] A. Manzonni, H. Daoud, R. Völkl, U. Glatzel, N. Wanderka, *Ultramicroscopy* **2013**, *132*, 212.
- [45] F. R. de Boer, *Cohesion in Metals: Transition Metal Alloys*, North Holland, Amsterdam **1988**.
- [46] L. Zhou, M. K. Miller, P. Lu, L. Ke, R. Skomski, H. Dillon, Q. Xing, A. Palasyuk, M. R. McCartney, D. J. Smith, S. Constantinides, R. W. McCallum, I. E. Anderson, V. Antropov, M. J. Kramer, *Acta Mater.* **2014**, *74*, 224.
- [47] H. C. Graham, H. H. Davis, *J. Am. Ceram. Soc.* **1971**, *54*, 89.
- [48] E. L. Creamer, I. Rozalsky, W. J. Lochmann, *Corrosion* **1967**, *23*, 297.
- [49] D. Lindberg, R. Backman, P. Chartrand, *J. Chem. Thermodyn.* **2007**, *39*, 1001.